ARTICLES

Drag Reduction in Aqueous Poly(ethylene oxide) Solutions Based on Drop Impact Images

Edvaldo Sabadini* and Melissa I. Alkschbirs

Instituto de Química, Universidade Estadual de Campinas, Caixa Postal 6154, CEP 13084-862, Campinas, Brazil

Received: April 29, 2003; In Final Form: October 21, 2003

The presence of very small amounts (ppm) of high molecular weight polymers in a solution produces high levels of drag reduction in a turbulent flow. This phenomenon, often termed as the Toms Effect, is highly dependent not only on molecular weight (MW) but also on the flexibility of the macromolecular chain. This paper describes the effects of poly(ethylene oxide) MW, concentration, and chain compaction on the impact structures produced during collision between a droplet against a shallow liquid surface (splash), both liquids containing the polymer. The impact energy stored in the splash structures (composed of crown, cavity, and Rayleigh jet) was estimated using a simple model and some morphological parameters obtained from instantaneous images of the splash. It was observed that the height of the Rayleigh jet, a liquid column produced from the collapse of the crown and the cavity, is highly sensitive to the elongational viscosity of the solution.

Introduction

When a fluid moves relative to a solid surface, a force is exerted on the surface in the direction of the motion, which is called drag force. Frictional drag results in dissipation of energy and, for many years, scientists and technologists have attempted to devise methods to minimize this effect. B. A. Toms found that a very dilute high-MW polymeric solution in a turbulent flow required a lower pipe flow-pressure gradient than the pure solvent to produce the same flow rate.[1] As a result of this pioneering work, the friction reduction by additives is often referred to as the "Toms Effect". Drag reduction (DR) levels may reach 80% in the laboratory.[2] Consequently, the phenomenon has become of considerable engineering interest, mainly in pumping processes.[3−6]

Macromolecular substances such as synthetics, biopolymers, or surfactants can produce the phenomenon described above.[3,4,7] However, poly(ethylene oxide), PEO, a flexible polymer is the most effective drag-reducing agent in aqueous systems.[4]

The model for DR in macromolecular systems is necessarily complex, as both turbulence effects and the extremely dilute nature of the solutions involved have to be taken into account.[3,8] Although the existence of DR has been recognized for many years, and the phenomenon is hydrodynamically well characterized, a molecular understanding of the role of added polymer in DR processes is still primitive.[9]

There are many different theories for the DR phenomenon, on the basis of molecular approach considerations. One theory assumes that the added macromolecules, under high shear, undergo a dynamic chain elongation, absorbing the energy of the eddies in the flow. This energy is then dissipated as elastic shear waves.[10,11] In this way, the macromolecules prevent both loss of fluid kinetic energy and the formation of eddies, resulting in DR.[4] Chain elongation occurs when the shear rate in a turbulent flow is greater than the reciprocal of the molecular relaxation time, $1/\tau$.[12,13] The relaxation time for a polymer in solution can be calculated from the Rouse[14] and Zimm[15] theories, in which both the MW and concentration of a polymer (C) are contributing factors, as shown in eq 1:

$$\tau = \frac{M_v(\eta_{sp}/C)\eta_0}{0.586RT\lambda_i} \quad (1)$$

where M_v, η_{sp}, η_0, R, T, and λ_i are the viscosity-averaged MW, the specific viscosity, the solvent viscosity, the gas constant, the absolute temperature, and the eigenvalues of Zimm Theory, respectively. Each λ_i is associated with one specific linear normal mode because of the cooperative motion of the polymer segments. A range of relaxation time is possible, but the longest where $\lambda_i = 1$ is the most important for DR.[10−12] Since η_{sp} depends on polymer concentration to a greater than the first power, τ increases with polymer concentration. Hence, the degree of DR is expected to increase with shear rate, MW, and concentration.[12]

Despite the great number of studies about DR, certain aspects are still not fully understood, for example, the influence of the pipe walls. Experimentally, the studies involving this phenomenon are generally performed during pipe flow, when levels of DR are related to the magnitude of the pressure drop along the tube. Recently, studies of DR have been focused on the visualization of structures produced by splash in aqueous PEO solution.[16,17]

Splash is a term used for the formation of a crownlike structure, produced by impact of a small liquid drop (primary drop) on a liquid surface (the target liquid).[18,19] The nature of splash formation depends on many different hydrodynamic

* Address correspondence to this author. E-mail: sabadini@iqm.unicamp.br.

10.1021/jp035158v CCC: $27.50
Published on Web 12/24/2003

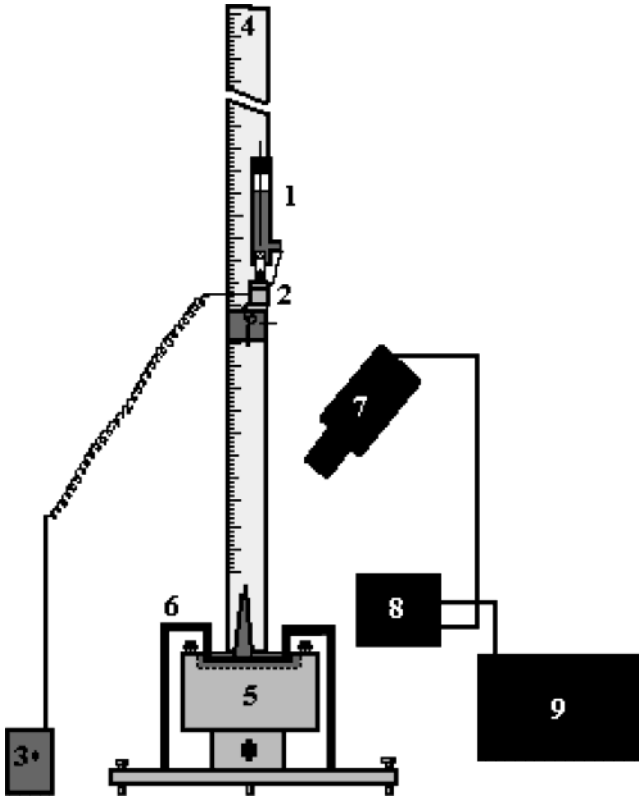

Figure 1. Scheme of the experimental apparatus used to obtain the images of controlled drop impact against a shallow liquid surface.

factors and some physicochemical characteristics specific to the fluid involved. In the milliseconds after droplet impact, the potential energy of the droplet provokes the formation of a "crown" on the liquid−air surface and a cavity in the target liquid. During the splash evolution, both the collapse of the crown and closing of the cavity force the liquid upward, forming a column called the Rayleigh jet.[20−22] The amplitude of the Rayleigh jet depends on the elongational viscosity of the solution and can be used to estimate the stored impact energy.[17]

This paper presents splash results for aqueous solutions of PEO, for a large range of MWs and concentrations. The effect of polymer compaction, because of the addition of K_2SO_4, on the elasticity of the solution, was also investigated. The energies of the crown, cavity, and Rayleigh jet were estimated using a simple model, allowing a discussion about the stored energy. The morphological parameters used in the model were obtained from "frozen images" captured using a high-speed CCD camera.

Experimental Section

Materials and Methods. The aqueous PEO solutions were prepared by an adaptation of the procedure suggested by Little and Wiegard.[23] Samples of PEO 1, 6, 9, 20, and 40×10^5 g·mol^{-1} (Aldrich), weighted within ±1 mg, were sprinkled over a large area of distilled deionized water to avoid clumping of the particles. At 3-h intervals, the solutions were gently stirred using a glass rod, to avoid polymer degradation. This procedure was also repeated on the following day. The final solutions were then prepared in volumetric flasks. For experiments involving polymeric solutions, the same concentration of PEO was used in both the droplet and the target solutions.

Apparatus Used To Produce the Splash. A schematic diagram of the experimental apparatus used in the splash studies is shown in Figure 1. A droplet of the solution under investigation is produced at the tip of a Teflon tube (∅ = 0.5 mm). This tube is connected to a reservoir of liquid, a Mariotte flask, producing a constant flow of liquid during droplet formation (1). A solenoid valve (Cole-Parmer Instrument Co., 3 way-valve, 1.5 W, 30 Psi) (2) is used to release droplets of mass 25 ± 2 mg. An electronic circuit (3) controls the solenoid valve. By positioning the valve at different increments along a ruler (4) (accurate to ± 0.1 cm) and hence altering the drop height, the gravitational potential energy of each drop can be varied if desired. Droplets for all the experiments were released 1.84 m from the surface of the target liquid. The impact vessel is a thermostatic tank, fixed to an elevator with a micrometric screw (5). A thin stainless steel plate, immersed in the target liquid, is fixed at the base of the apparatus by lateral arms (6). The depth of the liquid can therefore be adjusted by changing the height of the tank. The liquid film thickness (3.1 mm) was adjusted in each experiment.

Equipment for Capture of the Impact Images. The drop impact structures were captured using a Sony CCD DXC-9000 camera (7). A shutter speed of 1×10^{-4} s was used, set at 30 frames·s^{-1}. Two Halogen lamps (300W) (not shown in the scheme) were used to illuminate the impact region. The captured images were recorded on a tape recorder (Panasonic S-VHS Ag-1980) (8), interfaced with a computer (9), containing a frame grabber board (Media Cybernectic). Morphological parameters of the impact structures were obtained using software for image treatment, Image Pro-Plus 3.0. Averages of the morphologic parameters were obtained from 30 "frozen images" of each splash, and the error bars in the experimental data correspond to one standard deviation. The temporal evolution of each splash was obtained using a CCD camera (Red Lake, model PCI 8000s), at speed of 1000 frames·s^{-1}.

Viscosity, Surface Tension, and Density Measurements. The shear viscosity of the solutions was measured using an Ostwald viscometer-50. Surface tension measurements were taken using a tensiometer (Sigma 701 System Unit) and the Wilhelmy plate method. The density of the solutions was measured using a density meter (Anton Paar, DMA 58). All the experiments were conducted at 25 °C.

Results and Discussion

Morphology of the Impact. Figure 2 compares droplet impact sequence for (a) pure water and (b) aqueous PEO solution (40 ppm and MW 4×10^6 g·mol^{-1}), at progression of 0, 10, and 100 ms. To enable a direct comparison between the instant of drop impact and the maximum amplitude of the Rayleigh jet, the hydrodynamic conditions for both experiments were kept constant. What is noticeable from these images is the higher extension of the Rayleigh jet, and the lower fragmentation of the liquid column of the polymeric solution, compared to pure water.

The presence of polymer apparently has little effect on the crown morphology. However, a detailed analysis of both crowns at the time when they reach their maximum heights reveals important morphologic differences. The jets at the top of the crown for the PEO solution (Figure 3) are smoother and less fragmented than the jets for pure water (not shown). Secondary droplets are produced when the jets at the top of the crown reach the maximum amplitude. The capillary centripetal force overcomes its inertial force, creating capillary waves which travel back to the center of the jet column, creating droplets along of the jet.[24] The secondary drops are linked by a thick liquid filament, as a direct result of the viscoelastic behavior of PEO solutions.[25] The visualization of filaments has been used to determine the jets trajectories in splash experiments.[26] From

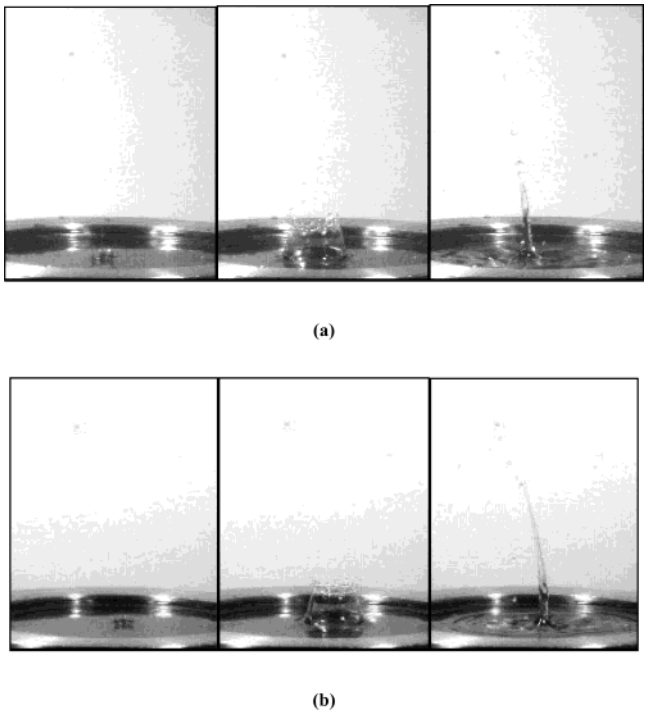

Figure 2. Comparative evolution for three stages (0 ms, 10 ms, 100 ms) for the splash in (a) pure water and (b) PEO aqueous solution (40 ppm, 4×10^6 g·mol^{-1}). The droplet was released at $h = 1.84$ m from the liquid impact surface. The depth of the impact liquid is 3.1 mm.

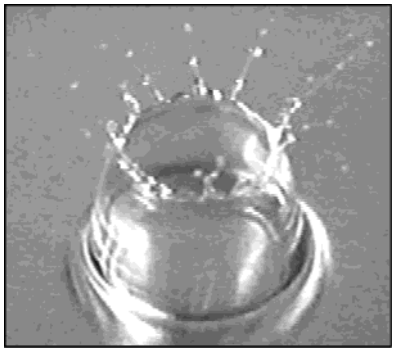

Figure 3. Photo in detail of a typical crown produced in an aqueous solution of PEO. A thick liquid filament joins the secondary droplets formed along the jets, at the top of the crown.

a practical point of view, addition of small amounts of a flexible polymer to herbicides reduces the loss of active agents during the impact of the solution against leaves.[27]

The collapse of the crown and the cavity starts approximately 20 ms after the impact of the primary drop and force a liquid column called as Rayleigh jet against gravitational force. Although understanding of splash is complex, the height of the Rayleigh jet depends, up to certain limits, on the impact energy stored. The maximum height of the jet is highly sensitive to PEO MW and concentrations. The authors proposed a relationship between the relative maximum amplitude for the Rayleigh jet produced in the pure solvent (H_{js}), and in the polymeric solution (H_{jp}), to enable an estimate of DR to be made for a system (eq 2):[17]

$$\%\mathrm{DR} = \left(1 - \frac{H_{js}}{H_{jp}}\right)100 \qquad (2)$$

This relationship is analogous to an equation used to estimate the %DR from the pressure drop in a pipe flow.[4] It has been observed that there is good agreement between results obtained from the drop collision experiments and conventional studies of DR.[17]

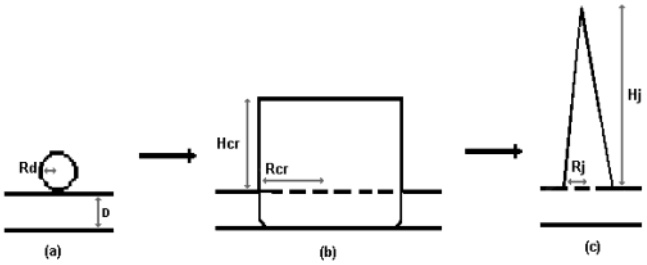

Figure 4. Schematic representation of three stages of the splash at the (a) moment of the impact; (b) maximum amplitude of the crown and cavity; and (c) maximum height of the Rayleigh jet.

The energy stored at different stages of the splash can be roughly estimated using a simple model, on the basis of energy conservation and a simplification of the impact structures geometry. In a first approach, the evolution of the splash can be analyzed by considering three stages (Figure 4): (a), the moment of impact; (b), the maximum amplitude of the crown and cavity; and (c), the maximum amplitude of the Rayleigh jet.

The drop impact energy (E_d), can be determined from the kinetic and potential energies (gravitational and surface), as expressed in eq 3:

$$E_d = mgh + mgR_d + 4\pi {R_d}^2\sigma \qquad (3)$$

where m, R_d are the mass and radius of the primary drop, respectively, σ is the surface tension, and h is the released height.

The crown can be considered to be a thin hollow liquid cylinder, and the Rayleigh jet a liquid cone. The energy necessary to create the crown (U_{cr}), the cavity (U_{cv}),[28] and the jet (U_j)[17] can be determined using eqs 4−6, respectively.

$$U_{cr} = {}^1/_2\pi g H_{cr}\rho \mathrm{D}{R_{cr}}^2 + 4\pi R_{cr}H_{cr}\sigma \qquad (4)$$

$$U_{cv} = {}^1/_2\pi g\rho D^2{R_{cv}}^2 + 2\pi R_{cv}D\sigma \qquad (5)$$

$$U_j = \frac{\pi}{3}\rho g{R_j}^2{H_j}^2 + \pi R_j[R_j + ({H_j}^2 + {R_j}^2)^{1/2}]\sigma \qquad (6)$$

where the first and second terms in the equations are the gravitational and surface energies, respectively; ρ is the density of the solution; D is the depth of the target liquid; R_{cr}, R_j, H_{cr}, and H_j are the radii and heights of the crown and jet. The cavity radius, R_{cv}, is assumed to be the same as the radius of the crown. All the R and H values were determined from "frozen pictures" of the splash in stages two and three. The disconnected droplets were not considered during determination of H_{cr} and H_j.

Equation 7 expresses the balance of energy required to produce the crown and the cavity:

$$E_d = U_{cr} + U_{cv} + W + E^* \qquad (7)$$

where W is the dissipated viscous energy and E^* represents other dissipative energies (as heat and sound).[29]

The density, shear viscosity, and surface tension for PEO solutions at the studied concentrations are close to the values for pure water, as shown in Table 1. For the experimental splash conditions used, $E_d \approx 4.5 \times 10^{-5}$ J. The average-morphological parameters, calculated energies for the crown, cavity, and Rayleigh jet for the splash both in water and PEO solution (40

TABLE 1: Density, Shear Viscosity, and Surface Tension Values for Some Aqueous Solutions of PEO, at 25 °C

PEO/10^5 g·mol^{-1}	concentration/ ppm	density/ g·mL^{-1}	shear viscosity/ cP	surface tension/ mN·m^{-1}
1	20	1.0719	0.893	62.54
6		1.0751	0.900	62.64
9		1.0721	0.902	62.59
20		1.0719	0.905	62.51
40		1.0716	0.910	62.32
1	40	1.0723	0.897	62.70
6		1.0720	0.907	62.56
9		1.0723	0.915	62.79
20		1.0724	0.925	62.76
40		1.0710	0.930	62.58
1	80	1.0715	0.903	62.89
6		1.0715	0.910	62.47
9		1.0722	0.930	62.65
20		1.0724	0.961	62.65
40		1.0710	0.964	62.68
1	100	1.0718	0.904	62.69
6		1.0715	0.931	62.41
9		1.0721	0.934	62.71
20		1.0723	0.981	62.53
40		1.0713	0.984	62.54

TABLE 2: Morphological-Average Parameters and Energies Obtained from the Splash in Pure Water and PEO Solution (40 ppm, 4 × 10^6 Gmol^{-1})

splash in	E_d/ 10^{-4}J	R_{cr}/ mm	H_{cr}/ mm	U_{cr}/ 10^{-4}J	U_{cv}/ 10^{-4}J	H_j/ mm	R_j/ mm	U_j/ 10^{-4}J
pure water	4.5	13.2	9.1	1.7 (38)[a]	0.4 (9)	23.6	3.4	0.8 (20)
PEO solution	4.5	13.7	8.5	1.8 (41)	0.5 (10)	49.8	3.6	3.9 (88)

[a] The values between the parentheses correspond to the percentage of the impact energy (E_d).

ppm, 4 × 10^6 g·mol^{-1}), are shown in Table 2. As R_{cr}, H_{cr} are similar for pure water and PEO solutions, there is almost no difference in the sum of the crown and cavity energies for both systems. Approximately 50% of the impact energy is stored in these structures, which is apparently independent of the presence of PEO. However, for the Rayleigh jet a dramatic difference is observed, with ≈20% of the impact energy being stored in the jet for pure water and ≈88% for a PEO solution. Despite the simplicity of the model used, the extra energy of the jet containing PEO is apparent. One possible explanation for this difference can be associated with term W in eq 7. This dissipative term can be estimated using eq 8,[28] which incorporates the rate of the crown or cavity formation:

$$W = 4\pi\eta \int_0^t D(dR_{cr}/dt)^2 dt \qquad (8)$$

Comparative diameter and height evolutions for the crown and cavity produced in pure water and a PEO solution (40 ppm and 4 × 10^6 g·mol^{-1}) are shown in Figure 5. The rates for the crown (term dR_{cr}/dt) and cavity formation are apparently independent of the addition of PEO and hence do not explain the difference in the energies of the jets. The difference can be instead associated with the degree of mixing of the drop and target liquids during the turbulent drop impact. This degree of mixture was estimated using experiments in which a dye is dissolved in the liquid of the primary drop, and the area of the resulting colored mark upon impact is measured immediately at the rest. The extent of mixing for pure water is almost twice that for an aqueous PEO solution (40 ppm of PEO 4 × 10^6 g·mol^{-1}).[16] Hence, the deformation of the target and drop liquids is more elastic for the PEO solution. For water, a significant fraction of the impact energy is dissipated during mixing of

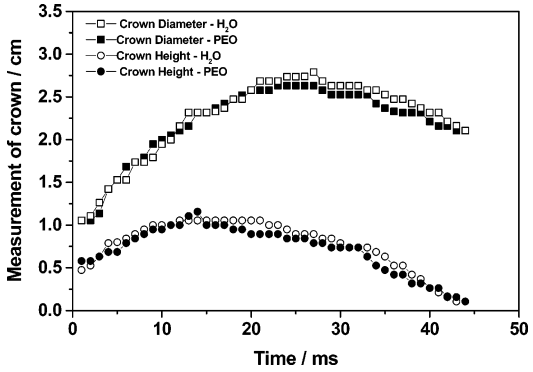

Figure 5. The dependence of the crown diameter and height in function of time for pure water and for a PEO solution (40 ppm, 4 × 10^6 g·mol^{-1}).

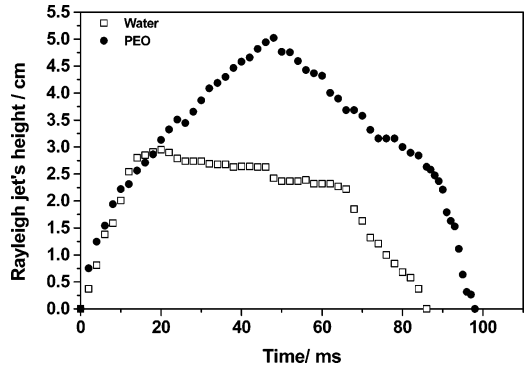

Figure 6. The dependence of the Rayleigh jet in function of time for pure water and for a PEO solution (40 ppm, 4 × 10^6 g·mol^{-1}).

the liquids in the turbulent flow. The relative elasticity of the PEO solution is shown by the comparative Rayleigh jet evolutions (Figure 6). The initial rate of jet formation is almost identical for both pure water and aqueous PEO solutions. However, the collapse of the jet for water begins at 20 ms, while the aqueous PEO jet stretches for at least 30 more milliseconds. The subsequent onset of effective contraction of the water jet takes 50 ms but is almost instantaneous for the PEO solution. Also, for the PEO system, the rate of jet contraction is almost the same as the rate of jet formation. This elastic behavior can be attributed to the high elongational viscosity of diluted high-MW PEO solutions.[30,31]

Typical elongation rate values during the splash can be estimated by considering, for example, cavity formation. The maximum cavity diameter (≈25 mm) is achieved in approximately 25 ms (Figure 5). Therefore, the rate of the cavity formation is ≈1 × 10^3 mm·s^{-1}. The thickness of the stretched cavity liquid can be assumed to be 0.15 mm (i.e., 1/2 D; this value is overestimated). The rate of elongation, ϵ, can be determined by $\epsilon = 1 \times 10^3$ mm·s^{-1}/0.15 mm ≈ 7000 s^{-1}. This value overcomes the onset value of a characteristic elongational flow for a diluted (4 × 10^6 gmol^{-1}) solution of PEO (≈3000 s^{-1}).[27] A high elongation rate is also observed for the formation and collapse of the Rayleigh jet for a PEO solution (jet formation velocity ≈1 × 10^{-3} mm·s^{-1}).

The present interpretation of Rayleigh jet elasticity is fundamentally based upon only bulk solution effects. However, the dilatational effects of the surface, because of the PEO adsorbed at the solution−air interface, should also be considered. Typically, the presence of PEO (in the studied range of concentrations) reduces the surface tension by approximately 10 mN·m^{-1} in relation to pure water (Table 1). The splash structures are produced so fast that it is possible to assume there

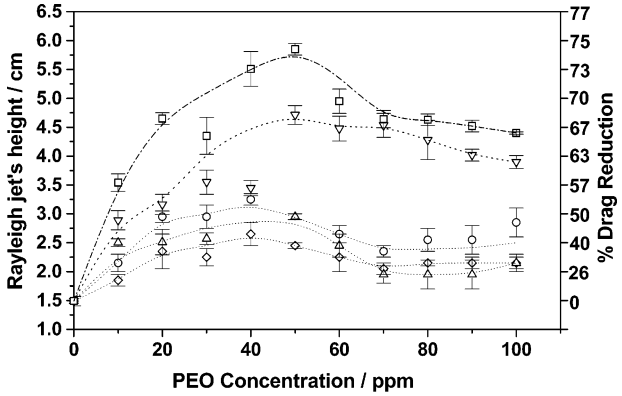

Figure 7. Dependence of the maximum height of the Rayleigh jet (and the percentage of DR) in function of PEO concentration: (◇) 1, (○) 6, (△) 9, (▽) 20, and (□) 40 × 10^5 g·mol^{-1}.

is no change in PEO concentration at the interface. In addition, large variation in the dynamic surface tension due to a diffusion of PEO to the interface is not expected. However, as observed by Scott et al., the presence of high-MW PEO at the interface increases the dilatational elasticity of the liquid−air interface comparatively with pure water.[32] The relative contribution of bulk and surface effects to the high elasticity of the Rayleigh jet in PEO solutions is an interesting area to be investigated.

Molecular Standpoint. Recently, the authors have demonstrated the dependence of the height of the Rayleigh jet with PEO MW and concentration.[17] In this work, a more complete study is presented (Figure 7). A gradual increase of PEO concentration produces a sharp increase in the maximum height of the Rayleigh jet. Beyond concentrations of PEO of 40−50 ppm, the height of the jet reduces, because of the dissipation of impact energy in the viscous flow, once the shear viscosity increases gradually for this range of PEO concentrations (Table 1). What is noticeable from this plot is the high elasticity of the jet produced for high-MW PEO solutions, for which ≈75% DR is achieved. The increase in DR as a function of PEO MW is in agreement with the model of Virk.[33] In this model, an increase of polymer gyration radius leads to an increase in DR, between certain limits.

The effect on drop impact of polymer and viscoelastic-surfactant solutions impacting against dry hydrophobic surfaces has been intensively studied.[27,34,35] When a drop of a dilute solution of a flexible polymer (bellow c^*) collides against a hydrophobic dry surface, the polymer chains stretch during the spreading of the liquid. Such extended conformation of the polymer coils result in a high local hydrodynamic viscosity, increasing the resistance for the liquid shrink back to the region of impact. Typically, the elongation rates for the solution during expansion and recoil are 6000 and 2500 s^{-1}, respectively. These studies provide significant insight into the fluid dynamics and the stretching−contraction motion of the polymer chain. This may allow us to propose a possible molecular model for motion of the PEO chains, to explain the high elasticity of the Rayleigh jet.

Table 3 shows the intrinsic viscosities for aqueous PEO systems and their respective longest relaxation time (calculated from eq 1). It is possible to conclude that for PEO with MW > 20 × 10^5 g·mol^{-1}, the deformation rates during the splash are higher than the onset rate for the chain stretching−contraction transition. The comparison of τ for high-MW PEO and the splash lifetime allow us to predict that the chains of PEO stretch during cavity and crown formation (in the first 25 ms after the drop impact) and that the maximum extension of the chain can be reached. During the collapse of these structures, high shear

TABLE 3: Intrinsic Viscosity for Some PEO in Aqueous Solution at 25 °C and Their Respective Longest Relaxation Time (λ_i = 1) Calculated Using the Zimm Equation

PEO-MW/ 10^5 g·mol^{-1}	intrinsic viscosity/dL·g^{-1}	relaxation time/ms
6	0.27	0.01
9	0.44	0.02
20	4.40	0.55
40	8.49	2.08
40/K_2SO_4, 0.5 mol L^{-1}	4.50	1.10

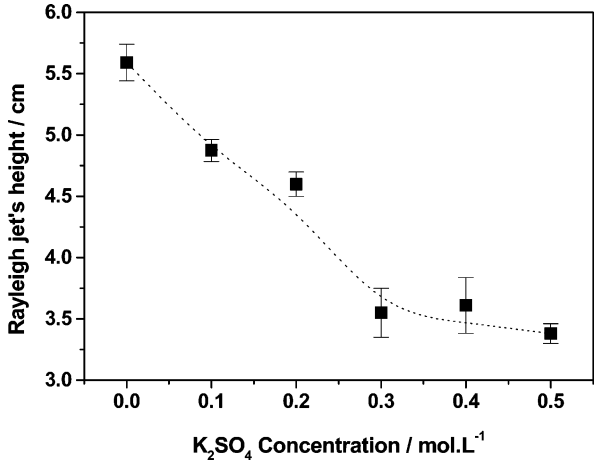

Figure 8. Dependence of the maximum height of the Rayleigh jet for aqueous solution containing PEO (40 ppm, 4 × 10^6 g·mol^{-1}) and K_2SO_4, in function of K_2SO_4 concentration.

rates can cause chain contractions (subsequent 25 ms). The PEO chains stretch again within the shear flow fields, developed during the approximately uniaxial flow regime produced in the Rayleigh jet. The high local hydrodynamic viscosity experienced by water molecules around the stretched PEO chains reduces not only the probability of eddies being created but also dissipates the energies of eddies produced as elastic shear waves. This reduces turbulence, resulting in high Rayleigh jet amplitudes, hence high levels of DR.

The compaction of PEO systems, because of the addition of K_2SO_4, on the elasticity of the Rayleigh jet was studied. Figure 8 shows the maximum height of the Rayleigh jet for aqueous solution containing PEO (40 ppm, 4 × 10^6 g·mol^{-1}) and K_2SO_4 in function of the K_2SO_4 concentration (from 0 to 0.5 mol·L^{-1}). It was observed that height of the jets for aqueous solution containing only K_2SO_4, in the studied concentration range, are close to the jet for pure water. The results clearly show a sharp decrease in the jet height for PEO solutions as a function of K_2SO_4 concentration. Beyond 0.3 mol·L^{-1} the jet amplitude is almost constant. This can be attributed to the proximity of the θ conditions for PEO (0.45 mol·L^{-1} of K_2SO_4 and 35 °C),[36] in which a maximum novel compaction is reached. The expansion factor, α, for PEO (4 × 10^6 g·mol^{-1}) was estimated by measuring the intrinsic viscosity of the solutions (Table 3). The results indicate that at 0.5 mol·L^{-1} of K_2SO_4 and 25 °C, $\alpha = ([\eta]/[\eta]_\theta)^{1/3} = 1.24$, meaning that the novel of PEO is approximately 24% more expanded in pure water. Even close to θ condition, PEO is able to produce DR in the range of 40%. As shown in Table 3, the values of τ for PEO near to the θ condition is approximately 50% lower than for PEO in pure water.

Conclusions

The presence of high-MW PEO in aqueous solutions dramatically alters the structures produced during drop impact against

a shallow solution surface, even at very low concentrations. It is possible that the chains of PEO stretch within the shear flow fields during formation of the crown and cavity and undergo contraction during collapse of these structures. The chains also stretch, during the formation of the Rayleigh jet, which is produced after the collapse of the crown and closing of the cavity. The high elongational viscosity of the polymer solutions reduces turbulence in the flow, as a result of the suppression of the energy in the eddies. This produces high levels of DR, illustrated by the high amplitudes of the jet. The Rayleigh jet itself is very sensitive to both PEO MW and concentration. Compaction of the PEO chains by addition of K_2SO_4 reduces the ability of the macromolecule to stretch, reducing the efficiency of the PEO as a drag-reducing agent.

Acknowledgment. The authors would like to thank Prof. Dr. Marcelo G. de Oliveira, Dr. J. C. Scott, and Sarah F. Anderson for useful comments and CNPq-PADCT and Fapesp for the financial support. M.I.A. wishes to thank Fapesp for the Research Fellowship.

References and Notes

(1) Virk, P. S.; Merrill, E. W.; Mickley, H. S.; Smith, K. A.; Mollo-Christensen, E. L. *J. Fluid Mech.* **1967**, *30*, 305.
(2) Leuchtag, H. R. *Phys. Today* **1978**, *31*, 17.
(3) McCormick, C. L.; Hester, R. D.; Morgan, S. E.; Safieddine, A. M. *Macromolecules* **1990**, *23*, 2132.
(4) Bailey, F. E., Jr.; Koleske, J. V. *Poly(ethylene oxide)*; Academic Press: New York, 1976.
(5) Figueredo, R. C. R.; Sabadini, E. *Colloids Surf., A* **2003**, *215*, 77.
(6) Kulicke, W. M.; Grägem, H.; Kötter, M. *Drag reduction phenomenon with special emphasis on homogeneous polymer solutions − Polymer Characterization/Polymer Solutions*; Springer-Verlag: Berlin, 1989.
(7) Sellin, R. H. J.; Hoyt, J. W.; Scrivener, O. *J. Hydraul. Res.* **1982**, *20*, 29.
(8) Bonn, D.; Couder, Y.; van Dam, P. H.; Douady, S. *Phys. Rev. E* **1993**, *47*, R28.
(9) Kim, O.-K.; Choi, L.-S.; Long, T.; Yoon, T. H. *Polym. Commun.* **1988**, *29*, 168.
(10) Lumley, J. L. *Appl. Mech.* **1967**, *20*, 1139.
(11) Peterlin, A. *Nature* **1970**, *227*, 598.
(12) Kim, O.-K.; Choi, L. S.; Long, T.; McGrath, K.; Armistead, J. P.; Yoon, T. H. *Macromolecules* **1993**, *26*, 379.
(13) Shenoy, A. V. *Colloid Polym. Sci.* **1984**, *262*, 319.
(14) Rouse, P. E. *J. Chem. Phys.* **1953**, *21*, 1272.
(15) Zimm, B. H. *J. Chem. Phys.* **1956**, *24*, 269.
(16) Sabadini, E.; Alkschbirs, M. I. *J. Visualization* **2001**, *4*, 217.
(17) Sabadini, E.; Alkschbirs, M. I. *Exp. Fluids* **2002**, *33*, 242.
(18) Worthingon, A. M. *Proc. R. Soc. A* **1882**, *188*, 217.
(19) Cossali, G. E.; Coghe, A.; Marengo, M. *Exp. Fluids* **1997**, *22*, 463.
(20) Hobbs, P. V.; Kezweeny, A. J. *Science* **1967**, *155*, 1112.
(21) Hobbs, P. V.; Osheroff, T. *Science* **1967**, *158*, 1184.
(22) Macklin, W. C.; Hobbs, P. V. *Science* **1969**, *166*, 107.
(23) Little, R. C.; Wiegard, M. *J. Appl. Polym. Sci.* **1970**, *14*, 409.
(24) Mourougou-Candoni, N.; Prunet-Foch, B.; Legay, F.; Vignes-Aadler, M.; Wong, K. *J. Colloid Interface Sci.* **1997**, *192*, 129.
(25) Goldin, M.; Yerushalmi, J.; Pfeffer, R.; Shinnar, R. *J. Fluid Mech.* **1969**, *38*, 689.
(26) Hoyt, J. W. *Flow Visualization − Fluid Engineering Division (ASME)* **1989**, 81.
(27) Bergeron, V.; Bonn, D.; Jean-Yves, M.; Vovelle, L. *Nature* **2000**, *405*, 772.
(28) Macklin, W. C.; Metaxas, G. J. *J. Appl. Phys.* **1976**, *47*, 3963.
(29) Prosperetti, A.; Oguz, H. *Annu. Rev. Fluid Mech.* **1993**, *25*, 577.
(30) Mun, R. P.; Byars, A. J.; Boger, D. V. *J. Non-Newtonian Fluid Mech.* **1998**, *74*, 285.
(31) Cheny, J. M.; Walters, K. *J. Non-Newtonian Fluid Mech.* **1999**, *86*, 185.
(32) Scott, J. C.; Stephens, W. B. *J. Acoust. Soc. Am.* **1972**, *52*, 871.
(33) Virk, P. S. *AIChE J.* **1975**, *21*, 625.
(34) Richard, D.; Clanet, C.; Quéré, D. *Nature* **2002**, *417*, 811.
(35) Cooper-White, J. J.; Crooks, R. C.; Boger, D. V. *Colloids Surf., A* **2002**, *210*, 105.
(36) *Polymer Handbook*, 2nd ed.; Brandrup, J., Immergut, E. H., Eds.; John Wiley & Sons: New York, 1974.